HHS Public Access

Author manuscript

Int J Dev Neurosci. Author manuscript; available in PMC 2016 November 01.

Published in final edited form as:

Int J Dev Neurosci. 2016 November ; 54: 32–38. doi:10.1016/j.ijdevneu.2016.08.004.

Regional Variation of White Matter Development in the Cat Brain Revealed by Ex Vivo Diffusion MR Tractography

Guangping Dai[1,2,‡,*], **Avilash Das**[3,4,*], **Emiko Hayashi**[3,†], **Qin Chen**[1,2,§], and **Emi Takahashi**[2,3,5]

[1]Department of Radiology, Harvard Medical School, Boston MA, USA

[2]Athinoula A. Martinos Center for Biomedical Imaging, Massachusetts General Hospital, Charlestown, MA, USA

[3]Division of Newborn Medicine, Department of Medicine, Children's Hospital Boston, Harvard Medical School, Boston MA, USA

[4]Medical Sciences in the College of Arts and Sciences, Boston University, Boston MA, USA

[5]Fetal-Neonatal Neuroimaging and Developmental Science Center, Boston MA, USA

Abstract

Three-dimensional reconstruction of developing fiber pathways is essential to assessing the developmental course of fiber pathways in the whole brain. We applied diffusion spectrum imaging (DSI) tractography to five juvenile ex vivo cat brains at postnatal day (P) 35, when the degree of myelination varies across brain regions. We quantified diffusion properties (fractional anisotropy [FA] and apparent diffusion coefficient [ADC]) and other measurements (number, volume, and voxel count) on reconstructed pathways for projection (cortico-spinal and thalamo-cortical), corpus callosal, limbic (cingulum and fornix), and association (cortico-cortical) pathways, and characterized regional differences in maturation patterns by assessing diffusion properties. FA values were significantly higher in cortico-cortical pathways within the right hemisphere compared to those within the left hemisphere, while the other measurements for the cortico-cortical pathways within the hemisphere did not show asymmetry. ADC values were not asymmetric in both types of pathways. Interestingly, tract count and volume were significantly larger in the left thalamo-cortical pathways compared to the right thalamo-cortical pathways. The bilateral thalamo-cortical pathways showed high FA values compared to the other fiber pathways. On the other hand, ADC values did not show any differences across pathways studied. These results demonstrate that DSI tractography successfully depicted regional variations of white matter tracts during development when myelination is incomplete. Low FA and high ADC values in the

Corresponding author: Emi Takahashi, Ph.D., Division of Newborn Medicine, Department of Medicine, Boston Children's Hospital, Harvard Medical School, 1 Autumn St. #456, Boston, MA 02115, USA, Athinoula A. Martinos Center for Biomedical Imaging, Fetal-Neonatal Brain Imaging and Developmental Science Center, Phone: 617-999-4033, emi@nmr.mgh.harvard.edu, Emi.TakahashiOki@childrens.harvard.edu.

*These authors equally contributed to this work.

‡Current address: Advanced Instrumentation Specialist, Science Center, Wellesley College, Wellesley, MA, USA.

†Current address: Medical Science Division, Tokai University Institute of Innovative Science and Technology, Kanagawa, Japan.

§Current address: Department of Neurology, West China Hospital, Sichuan University, Chengdu, Sichuan, China.

cingulum bundle suggest that the cingulum bundle is less mature than the others at this developmental stage.

Keywords

Development; White Matter; Diffusion Imaging; Tractography; Cat

Introduction

By virtue of the recent technical advances in diffusion-tensor magnetic resonance imaging (DTI), we can study global fiber pathways in the brain (Basser et al., 1994, 2000; Pierpaoli et al., 1996; Cellerini et al., 1997; Makris et al., 1997; Mori et al., 1999; Jones et al., 1999; Conturo et al., 1999). However, standard diffusion tractography (based on diffusion tensor imaging or DTI) tends to terminate in brain areas with low water diffusivity, indexed by low diffusion fractional anisotropy (FA), which can be caused by crossing fibers as well as by fibers with less myelin. For this reason, DTI tractography is not effective for delineating the structural changes that occur in the developing brain, where the process of myelination is incomplete.

High-angular resolution diffusion imaging (HARDI) including DSI has been proposed as an alternative to diffusion tensor imaging (DTI) for improved angular resolution of crossing fiber pathways (Tuch et al., 2003, Wedeen et al., 2008). HARDI is effective for delineating the structural changes that occur in developing fetal (preterm) brains (e.g. Takahashi et al., 2010, 2011, 2012), in which the process of myelination is incomplete, and in which crossing fibers are likely to exist in greater numbers than in the adult brain (Innocenti and Price 2005). We applied DSI tractography to immature cat brains to provide whole-brain 3-dimensional visualization of developing fiber systems (Takahashi et al., 2010), and correlated the resulting tractography with histology (Takahashi et al., 2011).

Many *ex vivo* diffusion studies of developing animal (Zhang et al., 2003, 2005; Huang et al., 2006; Kroenke et al., 2007; Huang et al., 2008; D'Arceuil et al., 2008; Kuo et al., 2008; Takahashi et al., 2010) and fetal human brains (Huang et al., 2009) have been published. These studies reported that FA values increase in the white matter with age. Some investigators have also performed diffusion tractography (Zhang et al., 2003; Kim et al., 2003; Huang et al., 2006; D'Arceuil et al., 2008; Huang et al., 2009; Takahashi et al., 2010) showing the development of major white matter pathways. However, these studies do not illustrate the detailed cortical fiber pathways in relation to the transient layer structures, probably because of the existence of low FA areas, crossing fibers, and regions where fibers take sharp turns (almost 90 degrees) as they enter the cortex. All of these factors can result in inappropriate termination of fiber tracking.

Histological and diffusion tractography studies show that, in humans, the process of myelination continues from infancy to adulthood (Richardson, 1982; Nomura et al., 1994; Hüppi et al., 1998). Similarly, cats undergo an extended period of postnatal white matter maturation. As we showed in our previous research (Takahashi et al., 2010, 2011), myelination in the cat brain already begins in some brain areas but is not fully complete at

postnatal day 35 (P35). We did not detect myelin in the white matter at P0 but fully detected them at P100. The degree of myelination in the white matter therefore varies in the cat brain at P35. Previously we studied overall white matter fiber development of the cingulum, thalamocortical, and two other association pathways in cats (at P0, P35, P75, and P100) without any quantification (Takahashi et al., 2010), and then focused on cortical fiber development in the same age range (Takahashi et al., 2011). These two past research studies used only one or two brains in each time point. Motivated by the past observations, in this study, we imaged five cat brains ex vivo at P35, and quantified diffusion properties (fractional anisotropy; FA, and apparent diffusion coefficient; ADC) on reconstructed tractography pathways for projection (cortico-spinal and thalamo-cortical), corpus callosum, limbic (cingulum and fornix), and association (cortico-cortical) fibers, to characterize regional differences in the degree of myelination.

Materials and Methods

Specimens

We performed scans on the brains of five juvenile kittens (P35), obtained from a group involved in vision research. After the cats were euthanized, their brains were perfused with phosphate-buffered saline solution followed by 4% paraformaldehyde, removed from the cranium, and fixed in 4% paraformaldehyde containing 1 mM gadolinium (Gd-DTPA) MRI contrast agent for 1 week to reduce the T1 relaxation time while ensuring that enough T2-weighted signal remained. For MR image acquisition, the brains were placed in the Fomblin solution (Fomblin Profludropolyether; Ausimont). We used a 4.7T Bruker Biospec MR system.

Scan Parameters

The pulse sequence used for image acquisition was a 3D diffusion-weighted spin-echo echo-planar imaging sequence, repetition time 1000ms, echo time 40 ms, with an imaging matrix of 96×112×128 pixels. Spatial resolution was 420×420×420μm. We performed diffusion spectrum encoding as previously described (Wedeen et al. 2005). Briefly, we acquired 515 diffusion-weighted measurements, corresponding to a cubic lattice in q-space contained within the interior of a ball of maximum radius bmax = 40,000 s/mm^2, with δ = 12.0 ms, Δ = 24.2 ms. The total acquisition time was 18.5 h for each experiment.

Diffusion Data Analyses—DSI Reconstruction

DSI reconstruction was performed using Diffusion Toolkit (http://trackvis.org), based on the Fourier relationship of the attenuated echo signal in q-space E(q) and the average diffusion propagator of the water molecular diffusion Ps (R):

$$E(q)=\int P_{\mathrm{s}}(R,\Delta)\exp(\mathrm{i}2\pi qR)\mathrm{d}R,$$

where R is the relative displacement of water molecule diffusion during the diffusion time D. Based on this calculation, applying a 3D Fourier transform to the echo signal over the q-space lead us to obtain the 3D probability density function (PDF) and then allowed us to map the fiber orientations (Lin et al. 2003; Wedeen et al. 2005). The transformation from q-

space signal to PDF values was performed voxel-by-voxel. To visualize the PDF, we integrated the second moment of PDF along each radial direction to acquire the orientation distribution function (ODF). In this study, we reconstructed the ODF within each voxel by interpolating along 181 radial directions, as calculated from the vertices of a regular and triangular mesh of the unit sphere surface. By comparing the length of each vector with the lengths of its neighboring vectors, we could obtain the orientational local maxima to represent intravoxel fiber orientations. We normalized all ODFs by the maximum ODF length within each voxel and calculated FA from orientation vectors by fitting the data to the usual tensor model.

Diffusion Data Analyses—Tractography

We used a streamline algorithm for diffusion tractography (Mori et al., 1999) described in previous publications (Takahashi et al., 2011, 2012). The term “streamline” refers to the fact that we connect tractography pathways using local maximum or maxima. This is true for both DTI and HARDI. The streamline technique is limited in its ability to resolve crossing pathways when used with the traditional DTI technique, because one simply connects the direction of the principal eigenvector on a tensor to produce the DTI tractography pathways. This is a recognized limitation of DTI, as discussed in the DTI paper of Mori et al. (1999). For this reason, in the current study, we used DSI, which detects multiple local maxima on an ODF (orientation distribution function). We used all the local maxima to produce DSI tractography pathways, thus enabling us to identify crossing pathways within a voxel. Trajectories were propagated by consistently pursuing the orientation vector of least curvature. We terminated tracking when the angle between 2 consecutive orientation vectors was greater than the given threshold (35 degrees) or when the fibers extended outside the brain surface, by using mask images of the brains created by MRIcro (http://cnl.web.arizona.edu/mricro.htm) for each specimen.

In many tractography studies, FA values are used to terminate fibers in the gray matter, which, in adults, has lower FA values than the white matter. However, as one of the objectives of our study was to detect fibers in low FA areas, we used brain mask volumes to terminate tractography fibers without using the FA threshold for tractography. Trajectories were displayed on a 3D workstation (TrackVis, http://trackvis.org).

The color coding of fibers is based on a standard RGB code, applied to the vector between the endpoints of each fiber. Mean FA, mean ADC, number, volume, and voxel count of each identified pathway were obtained through TrackVis.

Diffusion Data Analyses—ROI Placement and Restriction Parameters

Pathways in the whole brain, short cortico-cortical pathways within the left or right hemisphere, corpus callosum, fornix, cingulum, cortico-spinal, and left and right thalamo-cortical pathways were identified (Figure 1). Short cortico-cortical pathways were gathered by isolating a hemisphere using a slice filter and a both end restriction scheme; short fibers were selected for by restricting the minimum length threshold to 4.35mm and the maximum length threshold to 17.2 mm. Corpus callosum fibers were obtained by placing ROI in the sagittal plane and selecting against non-callosal fibers. Callosal fibers were separated into

anterior, superior, and posterior tracts based on the primary direction of fibers. Both fornix and cingulum pathways were isolated by placing any part ROI at the terminal ends of the structures. Cortico-spinal tracts were selected by placing terminal ROI in both the brain stem and the frontal lobe. Thalamo-cortical fibers were found by placing an either end ROI in the thalamic lobe of each hemisphere. The resulting fiber pathways were separated into anterior, superior, and posterior radiations.

Statistical Procedures

A two tailed paired t-test for hemispheric asymmetry was performed on mean FA, mean ADC, number, volume, and voxel count of the cortico-cortical, cingulum, fornix, cortico-spinal, and thalamo-cortical pathways. Using Bonferonni's correction significance was set to $p < 0.00125$ ($p=0.05/40$ comparisons).

Two-tailed paired-t test with Bonferroni's correction for multiple comparisons were performed on the mean FA and ADC values of each identified pathway. After Bonferroni's correction, significant p-value was set to $p < 0.00096$ ($p < 0.05/52$ comparisons).

Results

Asymmetry in measures in within-hemisphere and thalamo-cortical pathways

We first examined hemispheric asymmetries of FA, ADC, tract count, voxel count, and volume of tractography pathways for all bilateral fiber pathways. Apart from thalamo-cortical pathways, no significant asymmetries were found in any pathways (as shown in Table 3). Interestingly, while the total thalamo-cortical pathways did not show asymmetry, the superior radiations did show significant differences in voxel count ($p=0.000122$) and volume ($p=0.0000983$).

FA and ADC values compared in all identified pathways

Given that the tract number, volume, and voxel count of each developing pathway can vary depending on those measurements in adults, and they do not necessarily indicate the degree of maturation of the pathways, only mean FA and mean ADC values were compared across all pathways identified. Using two-tailed paired-t test with Bonferroni's correction for multiple comparisons, we found that the right and left thalamo-cortical pathways showed higher mean FA values compared to pathways in the whole brain, cortico-cortical pathways within a hemisphere, anterior and superior corpus callosum, cingulum, and fornix. There were no significant differences in mean FA value between the thalamo-cortical pathways and the posterior corpus callosum, and between the thalamo-cortical and the cortico-spinal pathways. Mean ADC values did not show any significant differences among the studied pathways. All p-values are listed in Table 1. Detailed FA and ADC values are shown in Figure 2 with specific values and standard deviations given in Table 2. Left and right thalamo-cortical pathways showed high FA values compared to the other fiber bundles. On the other hand, ADC values did not show significant differences across pathways.

Discussion

Our current results demonstrate that DSI tractography successfully depicted regional variations of white matter tracts during development when myelination is incomplete. Specific high FA values on the bilateral thalamo-cortical pathways suggest that the thalamo-cortical pathways mature earlier than the others at this developmental stage.

Maturation of the thalamo-cortical pathways

It is hard to compare ages between cats and humans directly, but based on emerging horizontal fiber pathways in the cortex, a P35 cat may correspond to around 30 gestational weeks in humans (see discussion in Takahashi et al., 2011). However, considering the degree of myelination, it starts in cats before P20, whereas myelination in humans can be obvious much later than postnatal 1 month of age. In this stage of P35 in cats, overall white matter structures are evident, but myelination is still underway to construct mature brain connectivity. The observation that the thalamo-cortical pathways mature earlier than the cortico-cortical pathways is consistent with the literature that reported the developmental order of the thalamo-cortical and cortico-cortical pathways (e.g. Kostovic and Vasung, 2009), which is consistent with causal relationships between the two pathways (e.g. Kingsbury et al., 2002). However, it was unexpected, and interesting, that the thalamo-cortical pathways also mature earlier than limbic pathways. Given that the cat is known to have notably prominent visual systems compared to other species, our current results for the thalamo-cortical pathways may reflect a strong degree of maturation of the visual pathways through thalamo-cortical pathways in cats.

ADC values in post-mortem brains

While mean FA values were indicative of the degree of maturation of fiber pathways, mean ADC values did not show any developmental variability of immature fiber pathways in this study. ADC values have shown significant changes during development *in vivo*. However, it has been reported that ADC values vary and are not a reliable index for assessing tissue properties in post-mortem brains, due to the post-mortem duration before fixation and the duration of fixation. In the current study, the post-mortem duration would have had a minimal effect since the animals were perfused in the same condition, but the duration of fixation varied across several months.

Advantages and limitation of the current study

Ex vivo imaging can provide high spatial resolution with great signal to noise because we can do long scans on post-mortem specimens with almost no motion and susceptibility artifacts. High-field MRI scanners and the way in which we prepare postmortem brain specimens for MRI scans, with Gd-DTPA contrast agents and custom-made RF MRI coils that just fit the specimens, allow us to image very high-resolution fiber pathways in the brain. Such innovative methodology has enabled us to visualize detailed coherent and crossing structures in the developing brain, even in the areas with low myelination (Takahashi et al., 2011). Although the diffusion indices, particularly ADC values, are known to be affected by post-mortem conditions, in vivo diffusion tractography is still not as

reliable as ex vivo tractography and extracting ADC values on such less reliable pathways could be questionable.

In this study, we used DSI to accurately identify brain pathways in developing cat brains, with combining DTI-based measurements on the identified pathways. Several methods have been proposed to improve characterization of microstructural tissue property (e.g. Zhang et al., 2012) which may provide more accurate measures in future studies.

Although cat brains have many white matter pathways corresponding to human pathways, there are evolutionary and, therefore, developmental differences between cats and humans. In the current study, advantages are that experimental animals could be perfused in the same condition and we could perform reliable quantification analyses on multiple samples, which cannot be done in humans. Nevertheless, it could be said that HARDI has potential to detect developmental variability across regions/pathways.

Acknowledgments

This work was supported by the Eunice Shriver Kennedy National Institute of Child Health and Development (NICHD) (NIH R01HD078561, R21HD069001) (ET). This research was carried out in part at the Athinoula A. Martinos Center for Biomedical Imaging at the Massachusetts General Hospital, using resources provided by the Center for Functional Neuroimaging Technologies, NIH P41RR14075, a P41 Regional Resource supported by the Biomedical Technology Program of the National Center for Research Resources (NCRR), National Institutes of Health. This work also involved the use of instrumentation supported by the NCRR Shared Instrumentation Grant Program (NIH S10RR023401, S10RR019307, and S10RR023043) and a High-End Instrumentation Grant Program (NIH S10RR016811). We thank Kenichi Ohki for providing the specimens, and Joseph B. Mandeville and Allison C.R. Scott for technical assistance.

References

Basser PJ, Mattiello J, LeBihan D. Estimation of the effective self-diffusion tensor from the NMR spin echo. J Magn Reson B. 1994; 103:247–254. [PubMed: 8019776]

Basser PJ, Pajevic S, Pierpaoli C, Duda J, Aldroubi A. In vivo fiber tractography using DT-MRI data. Magn Reson Med. 2000; 44:625–632. [PubMed: 11025519]

Cellerini M, Konze A, Caracchini G, Santoni M, Dal Pozzo G. Magnetic resonance imaging of cerebral associative white matter bundles employing fast-scan techniques. Acta Anat (Basel). 1997; 158:215–221. [PubMed: 9394958]

Conturo TE, Lori NF, Cull TS, Akbudak E, Snyder AZ, Shimony JS, McKinstry RC, Burton H, Raichle ME. Tracking neuronal fiber pathways in the living human brain. Proc Natl Acad USA. 1999; 96:10422–10427.

D'Arceuil H, Liu C, Levitt P, Thompson B, Kosofsky B, de Crespigny A. Three dimensional high-resolution diffusion tensor imaging and tractography of the developing rabbit brain. Dev Neurosci. 2008; 30:262–275. [PubMed: 17962716]

Huang H, Zhang J, Wakana S, Zhang W, Ren T, Richards LJ, Yarowsky P, Donohue P, Graham E, zan Zijl PCM, Mori S. White and gray matter development in human fetal, newborn and pediatric brains. Neuroimage. 2006; 33:27–38. [PubMed: 16905335]

Huang H, Yamamoto A, Hossain MA, Younes L, Mori S. Quantitative cortical mapping of fractional anisotropy in developing rat brains. J Neurosci. 2008; 28:1427–1433. [PubMed: 18256263]

Huang H, Xue R, Zhang J, Ren T, Richards LJ, Yarowsky P, Miller MI, Mori S. Anatomical characterization of human fetal brain development with diffusion tensor magnetic resonance imaging. J Neurosci. 2009; 29:4263–4273. [PubMed: 19339620]

Hüppi PS, Maier ES, Peled S, Zientara GP, Barnes PD, Jolesz FA, Volpe JJ. Microstructural Development of Human Newborn Cerebral White Matter Assessed in Vivo by Diffusion Tensor Magnetic Resonance Imaging. Pediatric Research. 1998; 44:584–590. [PubMed: 9773850]

Innocenti GM, Price DJ. Exuberance in the development of cortical networks. Nat Rev Neurosci. 2005; 6:955–965. [PubMed: 16288299]

Jones DK, Simmons A, Williams SC, Horsfield MA. Non-invasive assessment of axonal fiber connectivity in the human brain via diffusion tensor MRI. Magn Reson Med. 1999; 42:37–41. [PubMed: 10398948]

Kim DS, Kim M, Ronen I, Formisano E, Kim KH, Ugurbil K, Mori S, Goebel R. In vivo mapping of functional domains and axonal connectivity in cat visual cortex using magnetic resonance imaging. Magn Reson Imaging. 2003; 21:1131–1140. [PubMed: 14725920]

Kingsbury MA, Lettman NA, Finlay BL. Reduction of early thalamic input alters adult corticocortical connectivity. Dev Brain Res. 2002; 138:35–43. [PubMed: 12234656]

Kroenke CD, Van Essen DC, Inder TE, Rees S, Bretthorst GL, Neil JJ. Microstructural changes of the baboon cerebral cortex during gestational development reflected in magnetic resonance imaging diffusion anisotropy. J Neurosci. 2007; 27:12506–12515. [PubMed: 18003829]

Kostovic I, Vasung L. Insights from in vitro fetal magnetic resonance imaging of cerebral development. Semin Perinatol. 2009; 33:220–33. [PubMed: 19631083]

Kuo LW, Chen JH, Wedeen VJ, Tseng WY. Optimization of diffusion spectrum imaging and q-ball imaging on clinical MRI system. Neuroimage. 2008; 41:7–18. [PubMed: 18387822]

Lin CP, Wedeen VJ, Chen JH, Yao C, Tseng WY. Validation of diffusion spectrum magnetic resonance imaging with manganese-enhanced rat optic tracts and ex vivo phantoms. Neuroimage. 2003; 19:482–495. [PubMed: 12880782]

Makris N, Worth AJ, Sorensen AG, Papadimitriou GM, Wu O, Reese TG, Wedeen VJ, Davis TL, Stakes JW, Caviness VS, Kaplan E, Rosen BR, Pandya DN, Kennedy DN. Morphometry of in vivo human white matter association pathways with diffusion-weighted magnetic resonance imaging. Ann Neurol. 1997; 42:951–962. [PubMed: 9403488]

Mori S, Crain BJ, Chacko VP, van Zijl PC. Three-dimensional tracking of axonal projections in the brain by magnetic resonance imaging. Ann Neurol. 1999; 45:265–269. [PubMed: 9989633]

Nomura Y, Sakuma H, Takeda K, Tagami T, Okuda Y, Nakagawa T. Diffusional Anisotropy of the Human Brain Assessed with Diffusion-Weighted MR: Relation with Normal Brain Development and Aging. Am J Neuroradiol. 1994; 15:231–238. [PubMed: 8192066]

Pierpaoli C, Jezzard P, Basser PJ, Barnett A, Di Chiro G. Diffusion tensor MR imaging of the human brain. Radiology. 1996; 201:637–648. [PubMed: 8939209]

Richardson, EP, Jr. Myelination in the human central nervous system. In: Haymaker, W.; Adams, RD., editors. Histology and histopathology of the nervous system. Springfield (IL): Thomas; 1984. p. 146-173.

Takahashi E, Dai G, Wang R, Ohki K, Rosen GD, Galaburda AL, Grant PE, Wedeen VJ. Development of cerebral fiber pathways in cats revealed by diffusion spectrum imaging. Neuroimage. 2010; 49:1231–1240. [PubMed: 19747553]

Takahashi E, Dai G, Rosen GD, Wang R, Ohki K, Folkerth RD, Galaburda AL, Wedeen VJ, Grant PE. Developing neocortex organization and connectivity in cats revealed by direct correlation of diffusion tractography and histology. Cerebral Cortex. 2011; 21:200–211. [PubMed: 20494968]

Takahashi E, Folkerth RD, Galaburda AL, Grant PE. Emerging cerebral connectivity in the human fetal brain: An MR tractography study. Cerebral Cortex. 2012; 22:455–464. [PubMed: 21670100]

Tuch DS, Reese TG, Wiegell MR, Wedeen VJ. Diffusion MRI of complex neural architecture. Neuron. 2003; 40:885–895. [PubMed: 14659088]

Wedeen VJ, Hagmann P, Tseng WY, Reese TG, Weisskoff RM. Mapping complex tissue architecture with diffusion spectrum magnetic resonance imaging. Magn Reson Med. 2005; 54:1377–1386. [PubMed: 16247738]

Wedeen VJ, Wang RP, Schmahmann JD, Benner T, Tseng WY, Dai G, Pandya DN, Hagmann P, D'Arceuil H, de Crespigny AJ. Diffusion spectrum magnetic resonance imaging (DSI) tractography of crossing fibers. Neuroimage. 2008; 41:1267–1277. [PubMed: 18495497]

Zhang H, Schneider T, Wheeler-Kingshott CA, Alexander DC. NODDI: practical in vivo neurite orientation dispersion and density imaging of the human brain. Neuroimage. 2012; 61:1000–16. [PubMed: 22484410]

Zhang J, Chen Y, Hardwick JM, Miller MI, Plachez C, Richards LJ, Yarowsky P, van Zijl PCM, Mori S. Magnetic resonance diffusion tensor microimaging reveals a role for Bcl-x in brain development and homeostasis. J Neurosci. 2005; 25:1881–1888. [PubMed: 15728827]

Zhang J, Richards LJ, Yarowsky P, Huang H, van Zijl PCM, Mori S. Three-dimensional anatomical characterization of the developing mouse brain by diffusion tensor microimaging. Neuroimage. 2003; 20:1639–1648. [PubMed: 14642474]

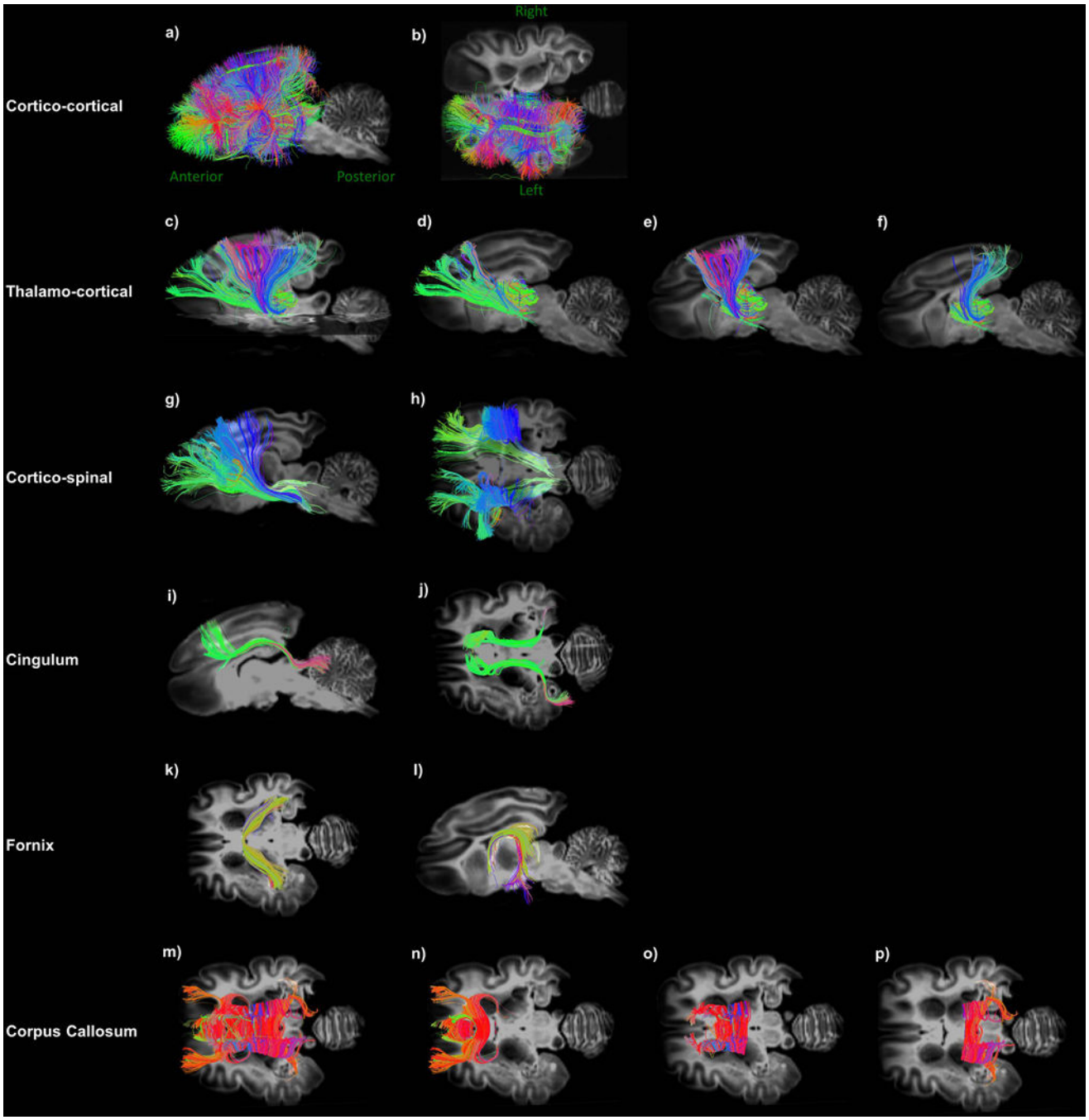

Figure 1.

Example tractography pathways for the corpus callosum, cingulum, fornix, and cortico-spinal pathways. (A) and (B) show cortico-cortical fibers in the left hemisphere. (C), (D), (E), and (F) show total, anterior, superior, and posterior thalamo-cortical fibers, respectively. (G) and (H) show cortico-spinal pathways. (I) and (J) show cingulum fibers, (K) and (L) show fornix pathways. (M), (N), (O), and (P) show total, anterior, superior, and posterior corpus callosum fibers, respectively.

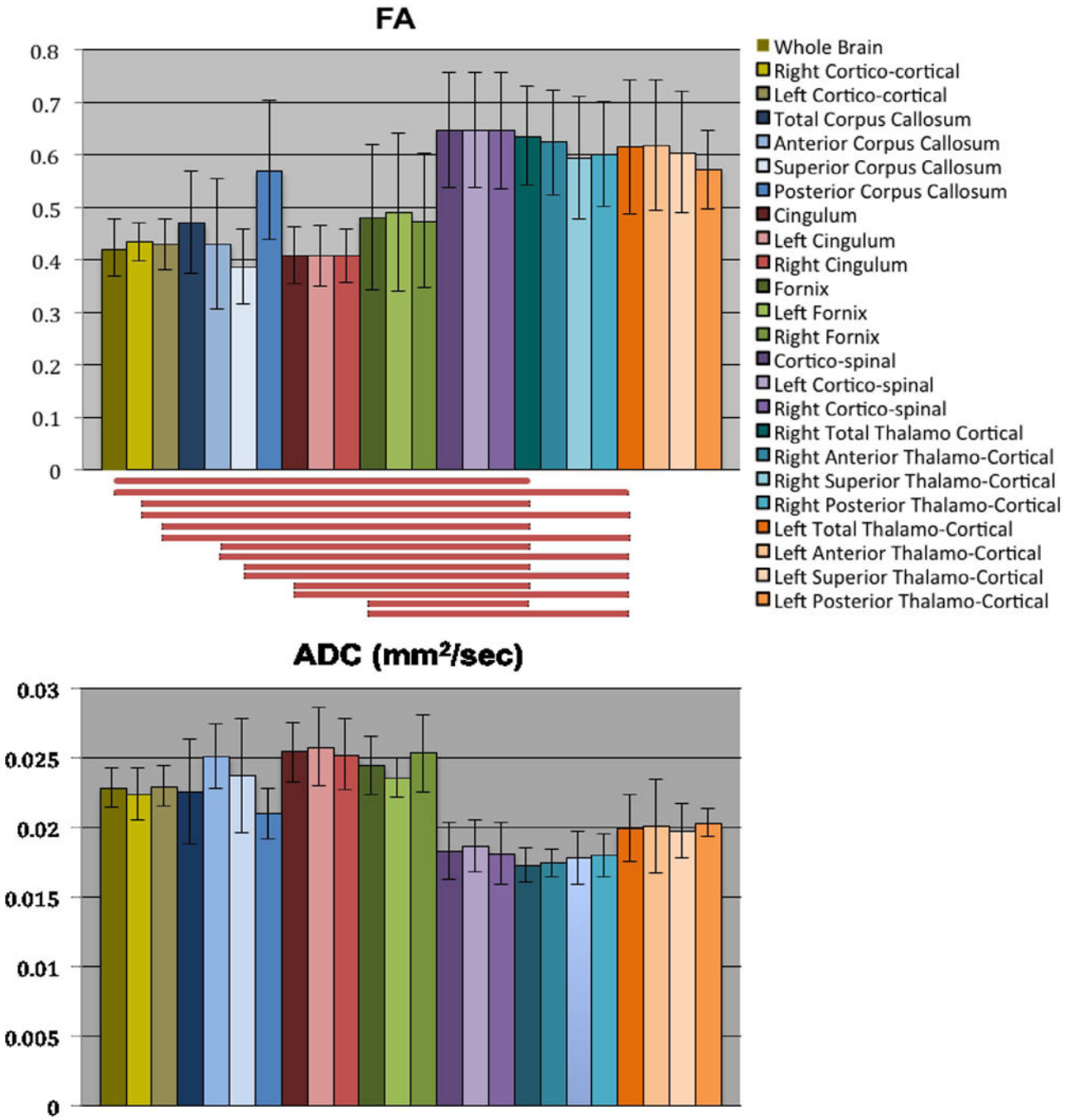

Figure 2.

FA and ADC values of identified tractography pathways. Error bars indicate standard deviation. Red lines below the FA panel indicate the pairs significantly different. There were no pairs significantly different in ADC.

Table 1

P-values resulting from t-test between: 1. whole brain and right cortico-cortical pathways, 2. whole brain and left cortico-cortical pathways, 3. whole brain and anterior corpus callosum pathways, 4. whole brain and superior corpus callosum pathways, 5. whole brain and posterior corpus callosum pathways, 6. whole brain and cingulum pathways, 7. whole brain and fornix pathways, 8. whole brain and cortico-spinal pathways, 9. whole brain and right thalamo-cortical pathways, 10. whole brain and left thalamo-cortical pathways, 11. right cortico-cortical and left cortico-cortical pathways, 12. right cortico-cortical and anterior corpus callosum pathways, 13. right cortico-cortical and superior corpus callosum pathways, 14. right cortico-cortical and posterior corpus callosum pathways,15. right cortico-cortical and cingulum pathways, 16. right cortico-cortical and fornix pathways, 17. right cortico-cortical and cortico-spinal pathways, 18. right cortico-cortical and right thalamo-cortical pathways, 19. right cortico-cortical and left thalamo-cortical pathways, 20. left cortico-cortical and anterior corpus callosum pathways, 21. left cortico-cortical and superior corpus callosum pathways, 22. left cortico-cortical and posterior corpus callosum pathways, 23. left cortico-cortical and cingulum pathways, 24. left cortico-cortical and fornix pathways, 25. left cortico-cortical and cortico-spinal pathways, 26. left cortico-cortical and right thalamo-cortical pathways, 27. left cortico-cortical and left thalamo-cortical pathways, 28. anterior corpus callosal and cingulum pathways, 29. superior corpus callosal and cingulum pathways, 30. posterior corpus callosal and cingulum pathways, 31. anterior corpus callosal and fornix pathways, 32. superior corpus callosal and fornix pathways, 33. posterior corpus callosal and fornix pathways, 34. anterior corpus callosal and cortico-spinal pathways, 35. superior corpus callosal and cortico-spinal pathways, 36. posterior corpus callosal and cortico-spinal pathways, 37. anterior corpus callosal and right thalamo-cortical pathways, 38. superior corpus callosal and right thalamo-cortical pathways, 39. posterior corpus callosal and right thalamo-cortical pathways, 40. anterior corpus callosal and left thalamo-cortical pathways, 41. superior corpus callosal and left thalamo-cortical pathways, 42. posterior corpus callosal and left thalamo-cortical pathways, 43. cingulum and fornix pathways, 44. cingulum and cortico-spinal pathways, 45. cingulum and right thalamo-cortical pathways, 46. cingulum and left thalamo-cortical pathways, 47. fornix and cortico-spinal pathways, 48. fornix and right thalamo-cortical pathways, 49. fornix and left thalamo-cortical pathways, 50. cortico-spinal and right thalamo-cortical pathways, 51. cortico-spinal and left thalamo-cortical pathways, 52. right thalamo-cortical and left thalamo-cortical pathways.

	FA	ADC		FA	ADC
1	0.653	0.969	27	0.000198	0.125
2	0.00282	0.972	28	0.0437	0.729
3	0.771	0.0509	29	0.402	0.501
4	0.282	0.693	30	0.0147	0.00836
5	0.0809	0.157	31	0.173	0.00632
6	0.723	0.642	32	0.0921	0.715
7	0.0491	0.707	33	0.544	0.00205
8	0.00339	0.209	34	0.00277	0.0618
9	0.000229	0.125	35	0.0157	0.00363
10	0.000261	0.123	36	0.0372	0.00887

	FA	ADC		FA	ADC
11	0.0341	0.997	37	0.000797	0.00161
12	0.906	0.0165	38	0.0000459	0.0895
13	0.142	0.431	39	0.425	0.191
14	0.0756	0.0796	40	0.000371	0.0119
15	0.677	0.621	41	0.0000814	0.201
16	0.0319	0.677	42	0.527	0.517
17	0.00431	0.214	43	0.135	0.868
18	0.000212	0.128	44	0.00712	0.16
19	0.000273	0.123	45	0.000603	0.096
20	0.905	0.0504	46	0.000889	0.137
21	0.218	0.678	47	0.0118	0.148
22	0.0717	0.0286	48	0.000302	0.0912
23	0.872	0.624	49	0.000677	0.0843
24	0.0228	0.682	50	0.554	0.651
25	0.00294	0.215	51	0.329	0.779
26	0.000177	0.128	52	0.347	0.444

Table 2

FA and ADC values of identified tractography pathways with standard deviations.

	FA	FA SD	ADC	ADC SD
Whole Brain	0.422	0.0537	0.0228	0.00141
Right Cortico-cortical	0.435	0.0351	0.0224	0.00184
Left Cortico-cortical	0.429	0.0473	0.0230	0.00144
Total Corpus Callosum	0.472	0.0968	0.0226	0.00375
Anterior Corpus Callosum	0.431	0.124	0.0252	0.00229
Superior Corpus Callosum	0.386	0.0709	0.0238	0.00406
Posterior Corpus Callosum	0.570	0.132	0.0211	0.00178
Cingulum	0.408	0.0531	0.0254	0.00212
Left Cingulum	0.409	0.0573	0.0258	0.00281
Right Cingulum	0.408	0.0504	0.0252	0.00256
Fornix	0.482	0.139	0.0245	0.00205
Left Fornix	0.490	0.151	0.0236	0.00140
Right Fornix	0.474	0.128	0.0254	0.00274
Cortico-spinal	0.648	0.111	0.0183	0.00203
Left Cortico-spinal	0.648	0.109	0.0187	0.00182
Right Cortico-spinal	0.647	0.110	0.0181	0.00219
Right Total Thalamo Cortical	0.636	0.0938	0.0173	0.00122
Right Anterior Thalamo-Cortical	0.624	0.0994	0.0174	0.00108
Right Superior Thalamo-Cortical	0.594	0.116	0.0178	0.00187
Right Posterior Thalamo-Cortical	0.600	0.101	0.0180	0.00153
Left Total Thalamo-Cortical	0.615	0.127	0.0199	0.00240
Left Anterior Thalamo-Cortical	0.618	0.123	0.0201	0.00336
Left Superior Thalamo-Cortical	0.604	0.116	0.0198	0.00193
Left Posterior Thalamo-Cortical	0.572	0.0740	0.0203	0.00103

Table 3

P-values resulting from t-tests for track count, voxel count, volume, FA, and ADC asymmetry in: 1. right and left cortico-cortical pathways, 2. right and left total thalamo-cortical pathways, 3. right and left anterior thalamo-cortical pathways, 4. right and left superior thalamo cortical pathways, 5. right and left posterior thalamo-cortical pathways, 6. right and left cingulum pathways, 7. right and left fornix pathways, 8.right and left cortico-spinal

	Track Count	Voxel Count	Volume	FA	ADC
1	0.297	0.831	0.844	0.0341	0.997
2	0.00305	0.0281	0.0117	0.347	0.444
3	0.496	0.978	0.980	0.549	0.576
4	0.00345	0.000122	0.0000983	0.428	0.580
5	0.134	0.0337	0.0311	0.680	0.296
6	0.345	0.745	0.976	0.531	0.683
7	0.834	0.627	0.338	0.336	0.514
8	0.0158	0.0181	0.0166	0.908	0.621